

A Lightweight Attention-based Deep Network via Multi-Scale Feature Fusion for Multi-View Facial Expression Recognition

Ali Ezati, Mohammadreza Dezyani, Rajib Rana, *Member, IEEE*, Roozbeh Rajabi, *Senior Member, IEEE*, and Ahmad Ayatollahi

Abstract—Convolutional neural networks (CNNs) and their variations have shown effectiveness in facial expression recognition (FER). However, they face challenges when dealing with high computational complexity and multi-view head poses in real-world scenarios. We introduce a lightweight attentional network incorporating multi-scale feature fusion (LANMSFF) to tackle these issues. For the first challenge, we have carefully designed a lightweight fully convolutional network (FCN). We address the second challenge by presenting two novel components, namely mass attention (MassAtt) and point wise feature selection (PWFS) blocks. The MassAtt block simultaneously generates channel and spatial attention maps to recalibrate feature maps by emphasizing important features while suppressing irrelevant ones. On the other hand, the PWFS block employs a feature selection mechanism that discards less meaningful features prior to the fusion process. This mechanism distinguishes it from previous methods that directly fuse multi-scale features. Our proposed approach achieved results comparable to state-of-the-art methods in terms of parameter counts and robustness to pose variation, with accuracy rates of 90.77% on KDEF, 70.44% on FER-2013, and 86.96% on FERplus datasets. The code for LANMSFF is available at <https://github.com/AE-1129/LANMSFF>.

Index Terms— Attention mechanism, Deep convolutional neural network, facial expression recognition, multi-level feature fusion

I. INTRODUCTION

Over the last three decades, facial expression has gained significant attention from researchers due to its powerful and universal nature, particularly in identifying emotions [1]. Ekman and Friesen [2] characterized six basic facial expressions (anger, disgust, fear, happiness, sadness, and surprise) on the basis of cross-cultural research. The study suggests that humans comprehend particular facial expressions similarly, irrespective of their culture. Distinct features of each facial expression distinguish it from other expressions; these features can be effectively acquired and identified by deep learning models. Deep networks have shown more robustness and effectiveness compared to traditional approaches, which often encounter difficulties in generalization to real-world environments [3]. In particular, Convolutional neural networks

(CNNs) have robust capabilities for extracting, learning, and classifying features. Due to these capabilities, CNNs are highly effective for identifying and discerning subtle variations in facial expressions [4].

However, facial expression recognition (FER) has faced challenges due to the high computational demands of CNNs and the presence of real-world situations. In the literature, few studies have systematically investigated how to reduce the number of trainable parameters in CNNs [5], [6]. A greater number of model parameters requires more training samples to avoid overfitting [7]. Although early CNN-based methods show promising recognition performance in constrained environments, they often have poorer accuracy in real-world scenarios [8]. Multi-view poses in unconstrained environments may cause alterations in facial areas of images, which complicate accurate classification [9]. Several studies [9], [10], [11], [12], [13], [14], [15] have utilized attention mechanisms and multi-scale features to improve recognition rates in such contexts. Hu et al. [13] introduced the squeeze-and excitation (SE) module to enhance channel relationships by recalibrating the significance of each channel. Convolutional block attention module (CBAM) [12] employs two consecutive stages of channel-wise and spatial-wise attention to refine features. Furthermore, Zhao et al. [14] obtained robust and diverse information through the utilization of multi-scale features.

To address the aforementioned issues, we propose a lightweight fully convolutional attention-based network called LANMSFF, which utilizes two novel modules: mass attention (MassAtt) and point-wise feature selection (PWFS). In MassAtt block, attention maps are generated simultaneously in both spatial and channel dimensions. This process reweights feature maps to highlight critical features while diminishing irrelevant ones. Another effective technique to improve recognition rates is to utilize multi-scale features, which provide robust and varied information in multi-view situations [14]. To this end, we utilize dilated convolutions and fusion of intermediate features to obtain multi-scale features. Many existing methods simply fuse features from various scale and assign identical weights to these features [14], [15]. However, utilizing all features from diverse perspectives without considering their importance may negatively impact recognition accuracy [16].

A. Ezati, MR. Dezyani and A. Ayatollahi are with the School of Electrical Engineering, Iran University of Science and Technology, Iran. E-mail: {aliezati, mohammadreza_dezyani}@elec.iust.ac.ir, ayatollahi@iust.ac.ir
R. Rana is with the School of Mathematics, Physics and Computing, University of Southern Queensland, Australia.

E-mail: rajib.rana@unisiq.edu.au

R. Rajabi is with the DITEN Department, University of Genoa, Italy.

E-mail: roozbeh.rajabi@unige.it

Therefore, we employ PWFS block to suppress weak multi-scale features before fusion. Our major contributions to this work can be summarized as follows:

- 1) A lightweight FCN-based model is proposed to strike a balance between accuracy and parameter counts. Moreover, this model handles multi-view pose scenarios.
- 2) MassAtt module is introduced to enable the model to focus on both channel and spatial attention maps simultaneously. By reweighting feature maps, this module highlights critical features while suppressing irrelevant ones.
- 3) PWFS block is designed to enhance efficiency of the model. This block reduced the number of parameters and selects powerful features before fusing them.
- 4) Experimental results demonstrate that the proposed method performs comparably to state-of-the-art (SOTA) on various key datasets, including KDEP [17], FER-2013 [18], and FERPlus [19]. Our method shows robustness to multi-view head poses while keeping parameter count optimal.

The remainder of the paper is organized as follows. Section II reviews literature on FER. Next, we describe the proposed models in Section III. Section IV describes the datasets and implementation details, followed by our experimental results. Finally, we conclude the paper in section V by giving insights for future studies.

II. RELATED WORK

A. Lightweight FER Models

CNNs have been getting deeper to achieve accuracy in various applications [4], [7]. However, these deep networks require powerful GPUs due to their high computational complexity. Several recent studies [10], [20] have focused on developing lightweight deep networks to mitigate these challenges.

Shao et al. [21] introduced a solution to overfitting and high computational complexity by introducing a CNN architecture. This architecture includes six modules of depth-wise separable residual convolution, followed by a global average pooling (GAP) layer. Each module consists of three depth-wise separable (DWS) [6] convolutional layers, a max pooling layer, and a standard convolution layer within a skip connection path. Gera et al. [20] utilized a lightweight facial recognition model called LightCNN [22] as a pre-trained backbone. They also adopted the efficient channel attention (ECA) mechanism [23] to reduce computational complexity. Jiang et al. [10] introduced the neuron energy-one shot aggregation (NE-OSA) block to reduce parameters. Unlike concatenating all previous features at each succeeding layer in DenseNet [24] approach, this block aggregates the feature maps of previous convolutional layers only once in the final feature map. In addition, they employed parallel efficient separable convolutions with multi-scale receptive fields on the input image to obtain feature maps at different scales. However, the parameter counts of these

methods still consist of a large number of parameters, which make them inappropriate for real-world applications. In contrast, we achieved comparable efficacy utilizing a lightweight FCN model with only a handful number of parameters.

B. Visual-attention Based FER

Attention in neural networks concentrates on the specific parts of input, disregarding irrelevant features. Visual attention-based networks are proposed for localizing crucial regions in computer vision tasks, such as FER.

Li et al. [25] proposed a FER system, which utilizes two CNN feature extractors to achieve feature maps from raw and local binary pattern (LBP) source images. Subsequently, these feature maps are utilized by an attention module to construct attention maps. After refining the feature maps with the attention module, the features undergo a dense convolutional module comprising four dilated convolutions before a classification module. Wang et al. [9] presented region attention network (RAN) in which CNN-based backbones capture features from multiple regions in the face. Following this, the framework utilizes two modules, namely self-attention and relation attention, to acquire attention weights for a compact face representation. Huang et al. [11] incorporated grid-wise attention to extract low-level features from distinct facial regions. These extracted features were subsequently fed into a CNN-based network, which collected pyramid feature maps at each convolutional layer and resized them to a fixed-length size. The resized feature maps were then utilized as tokens in a visual transformer, which ultimately extracted global features for FER tasks. Li et al. [26] proposed a strategy that incorporates both local and global features from sliding patches and the entire face, respectively. Subsequently, these features undergo SE attention modules to enhance feature representation. Similarly, Liu et al. [27] proposed a patch attention convolutional vision transformer (PACVT) in order to overcome the challenge of partial occlusion in the FER task. Inspired by CBAM, their backbone incorporates both channel and spatial attention. Gera et al. [20] partitioned the feature maps of a pre-trained CNN-based model into four non-overlapping patches to capture both local and global information. After passing these features through ECA modules to accentuate salient regions, an ensemble learning strategy is employed to enhance overall performance. Jiang et al. [10] introduced multi-path interactively squeeze and extraction attention (MPISEA) module to divide channel-wise feature maps from the stem module into two patches. These patches undergo linear transformations to generate subspaces. Following the application of dot products to these subspaces, a sigmoid function is utilized to generate an attention mask, which is finally multiplied with the input image. Due to the effectiveness of visual attention in these methods, we use attention mechanisms in both early and later blocks to incorporate low and high-level features into attention-based representations.

TABLE I
COMPARATIVE SUMMARY OF OUR STUDY AND PREVIOUS LITERATURE

Paper/Author (Year)	Method	Lightweight	Attention		Multi-scale fusion		Multiview
			Channel	Spatial	Direct	Constraint	Scenario
Shao et al.[21] (2019)	CNN	✓	✗	✗	✗	✗	✗
Wang et al. [9] (2020)	RAN	✗	✗	✓	✗	✗	✓
Li et al. [26] (2020)	SPWFA-SE	✗	✓	✗	✓	✗	✗
Liu et al. [30] (2021)	DML-Net	✗	✗	✗	✓	✗	✓
Huang et al. [11] (2021)	FER-VT	✗	✗	✓	✗	✗	✗
Gera et al.[20] (2022)	CERN	✓	✓	✗	✗	✗	✓
Liu et al.[27] (2023)	PACVT	✗	✓	✓	✓	✗	✗
Jiang et al. [10] (2023)	TST-RRN	✓	✓	✓	✓	✗	✗
Xiao et al.[16] (2023)	CFNet	✗	✗	✗	✗	✓	✗
Ma et al. [28] (2023)	VTFF	✗	✓	✓	✗	✓	✓
This paper (2024)	LANMSFF	✓	✓	✓	✓	✓	✓

C. Multi-scale Fusion

The complementary attributes of multi-perspective features have motivated several studies to integrate these types of features.

Li et al. [26] extracted local and global features from sliding patches and entire facial images, respectively. They fused these two types of features in a direct manner to obtain a synergistic outcome. Liu et al. [27] leveraged both global and local features by directly merging them via concatenation. After extracting feature maps using a CNN backbone, local features were obtained using a vision transformer to capture long-range dependencies between patches. Jiang et al. [10] utilized several parallel separable convolutions with multi-scale receptive fields to obtain multi-scale feature maps which were fused through element-wise addition. In contrast to the above-mentioned methods that adopted direct feature fusion, few approaches consider the importance of individual features before fusion. Xiao et al. [16] assigned adaptive weights based on their significance before fusing to enhance recognition rates in unconstrained conditions. Ma et al. [28] introduced attentional selective fusion (ASF) module to adaptively fuse LBP and CNN feature. ASF prioritizes discriminative features by assigning them greater weight, and the fusion weights are generated through a global-local attention mechanism. However, our work employs both direct fusion and constrained fusion. The latter is achieved through the elimination of redundant features prior to the fusion process.

D. Multi-view Scenarios

Real-world images of human faces are not always captured in frontal positions, which poses challenges for FER tasks since important facial regions may become disappeared in such conditions [29]. Liu et al. [30] employed three ResNet50 [31] models to extract features from distinct facial areas (eyes, mouth) as well as the entire face. These features were subsequently fused and mapped into three embedding features for a multi-task learning process. This process addressed the tasks of FER, pose estimation, and embedding distances. RAN [9] and CERN [20] proposed end-to-end learning models based on attention mechanism, wherein salient regions of facial images were emphasized, resulting in pose-robust models. Ma

et al. [28] proposed visual transformers with feature fusion (VTFF) model that exhibits promising generalization under pose-variant conditions. Following extraction and fusion of LBP and RGB features, VTFF transformed the fused features into sequences of visual words. These sequences were then utilized in a transformer architecture to learn the relation between them. All of these approaches exhibit a suitable degree of robustness to pose variation. Accordingly, we utilize an attention mechanism and feature selection to enhance the robustness against pose variation. Table I presents a brief comparison between existing literature and our work, dividing them into four broad categories: lightweight FER models, attention mechanisms, multi-scale fusion, and multi-view scenarios.

III. PROPOSED METHOD

A. Architecture Overview

We designed LANMSFF to achieve high accuracy while also minimizing the number of parameters. The model comprises four sequential blocks that share similarities between the first and third blocks, as well as between the second and fourth blocks (see Fig. 1).

The first and third blocks each initiate with three convolutional layers, with 66 channels in the first block and 78 channels in the third block. The first and third convolutional layers in these blocks are standard convolutions, whereas the second one is a DWS convolution to reduce computational complexity. After these convolutions, batch normalization (BN) is utilized to normalize activations and reduce overfitting. Subsequently, a max-pooling layer with a 2×2 kernel size and a stride of 2 is employed to decrease spatial dimensions. Finally, a dropout layer is introduced to enhance the learning of robust features by randomly removing some neurons during the training process.

The second block (with 72 channels) and the fourth block (with 84 channels) both begin with the shuffling and splitting module. This module adds randomness and divides the input feature maps into two groups based on channels. Then, the divided feature maps are directed into two parallel convolutional paths. One path employs three 3×3 convolutions

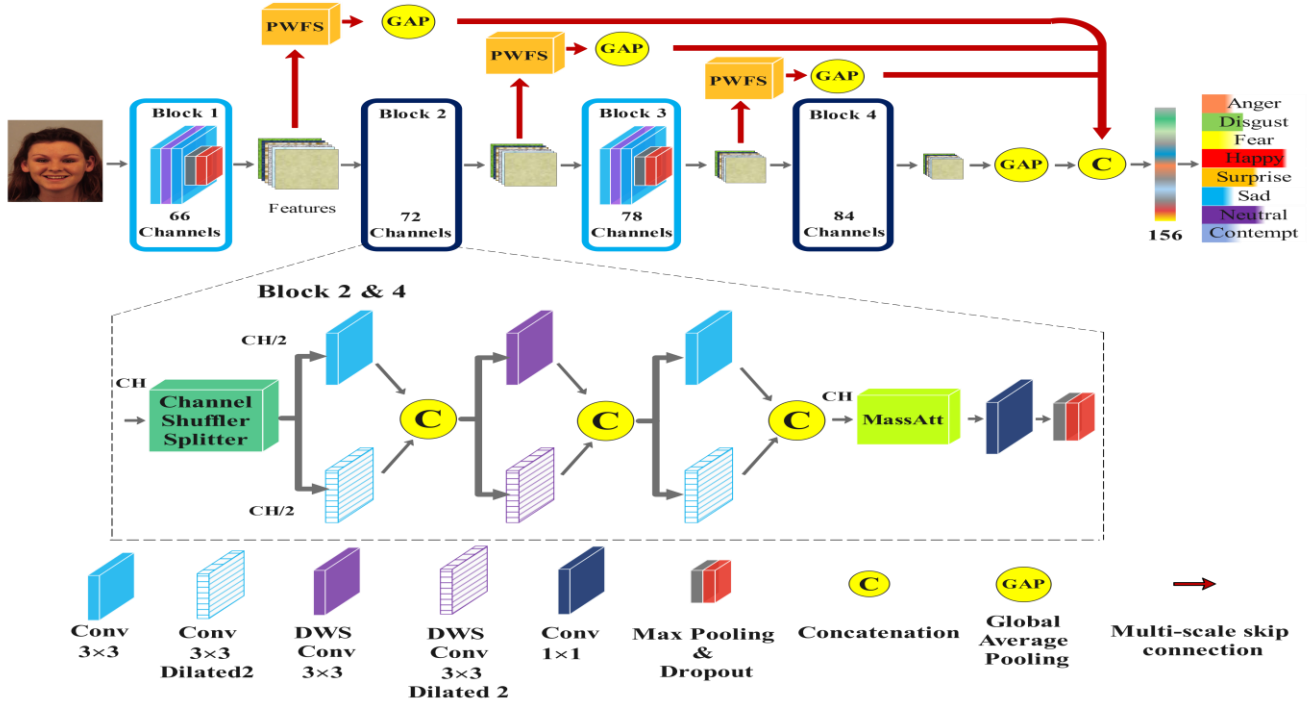


Fig. 1. The overview of our proposed model.

without dilation, whereas the second one utilizes three 3×3 dilated convolutions [32] with a dilation rate of two to reach a larger receptive field without additional parameters. Each convolutional path has a distinct receptive field, which enables it to capture a various type of feature. Features are concatenated in both paths after each convolution in order to integrate information across the two parallel groups. By integrating multi-scale features from both paths, the model's ability to recognize a wide range of spatial structures is enhanced, leading to improved generalization in challenging situations. Following that, a series of operations are performed on the outputs of the two branches: a MassAtt block, a 1×1 convolutional layer, batch normalization (BN), max pooling, and a dropout layer.

We integrate multi-level features into the classification procedure in order to improve gradient flow and alleviate the vanishing gradient issue during the training process. Specifically, the outputs of the first three blocks undergo PWFS blocks to remove the weakest one-third of features. Subsequently, GAP operations reduce the dimension of feature maps, preparing them for concatenation. The results of the fourth block and the GAP operations are then concatenated to generate a feature vector with 156 nodes. Finally, this vector is fed into a dense (classification) layer with neurons equal to the number of classes, which maps the extracted features to the corresponding expression label. The convolutional layers utilize rectified linear unit (ReLU), described as $f(z) = \max(z, 0)$. The dense layer computes the probability of each class using softmax activation function as follows:

$$\text{softmax}(z_i) = \frac{\exp(z_i)}{\sum_0^{n-1} \exp(z_i)} \quad (1)$$

where z_i is i -th class score, and n is the number of classes.

B. PWFS Block

numerous existing methods have employed fusion to directly leverage multi-scale features by allocating these features uniform weights [14], [15]. Fundamentally, the features extracted for direct fusion may contain redundant information that obscure crucial facial details. This issue becomes particularly evident in real-world conditions due to the inclusion of background regions containing redundant details. The presence of redundant information can pose challenges for in-the-wild FER applications and may deteriorate the FER system performance [33].

Inspired by the max feature map (MFM) approach [22], we introduce the PWFS block to eliminate weak features from each scale before fusion. This block reduces the parameter count, leading to a more efficient and compact architecture. Moreover, the generalization capabilities of CNNs are enhanced by the method's ability to extract more informative features from a relatively small number of feature maps.

As depicted in Fig. 2, the process of the PWFS block is initiated by examining the input feature maps denoted as $f = \{1, \dots, C\} \in R^{(H \times W)}$, where C , H , and W represent the number of feature channels, height, and width, respectively. Subsequently, the feature map is divided into three distinct sub-groups based on channels: S_0, S_1 , and $S_2 \in R^{\left(\frac{C}{3} \times H \times W\right)}$. Following this, the block preserves the highest and middle features as well as discarding the lowest ones across identical positions in the three sub-group feature maps. Then, the two remaining sub-group undergo a point-wise average process to squeeze them into a single sub-group. It is notable that the spatial dimension of the feature maps remains constant during

this process. The mathematical expression of this block is as follows:

$$v_{chw} = \frac{1}{2} \left(\max \left(x_{chw}^{s0}, x_{chw}^{s1}, x_{chw}^{s2} \right) + \text{mdn} \left(x_{chw}^{s0}, x_{chw}^{s1}, x_{chw}^{s2} \right) \right) \quad (2)$$

where X_{chw} represents an element located at position (h, w) within the c -th feature map of each respective sub-group, while v_{chw} corresponds to the resulting output of PWFS.

C. MassAtt Block

The MassAtt block applies attention mechanisms at both channel and spatial levels by adjusting the importance of feature maps, which is crucial in pose-variant FER.

As illustrated in Fig. 3, the schematic input-output sequence of MassAtt consists of two parallel paths. The upper attention path comprises a GAP layer and a bottleneck structure that generates a channel attention map, akin to SE attention mechanism. The GAP operation generates channel descriptors, which are then applied to the bottleneck structure that consists of two dense layers activated with ReLU and sigmoid functions, respectively. The first dense layer reduces dimensionality by a factor of 4, while the second one restores dimensionality to the dimension of the original input channel.

In the same way, the lower attention path attains the spatial attention map following the same procedure. This path initiates with the calculation of spatial descriptors along the channel axis by averaging the input feature maps in a point-wise GAP operation. subsequently, there are two convolutional layers with a stride of two to reduce the spatial dimensions, followed by two transposed convolutional layers that increase the dimensions to the original input size. In the final stage, both the channel and spatial attention maps are multiplied with the input feature map.

Mathematically, MassAtt block can be defined as follows:

$$\begin{cases} Y = X \otimes A_c \otimes A_s \\ A_c = \sigma(Z_1 \delta(Z_0 D_c)) \\ A_s = \sigma(Z_5 \delta(Z_4 \delta(Z_3 \delta(Z_2 D_s)))) \end{cases} \quad (3)$$

where X and Y represent the input and output feature maps, respectively. In addition, $A_c \in \mathbb{R}^{C \times 1 \times 1}$ and $A_s \in \mathbb{R}^{1 \times H \times W}$ denote the channel and spatial attention maps. Here \otimes , σ , and δ represent element-wise multiplication, sigmoid, and ReLU functions, respectively. The weights of dense layers are denoted as $Z_0 \in \mathbb{R}^{(C/r) \times C}$, $Z_1 \in \mathbb{R}^{C \times (C/r)}$. The weights of convolutional layers are represented by $Z_2 \in \mathbb{R}^{2 \times 1 \times 3 \times 3}$ and $Z_3 \in \mathbb{R}^{4 \times 2 \times 3 \times 3}$, while the weights of transposed convolutional layers are denoted as $Z_4 \in \mathbb{R}^{4 \times 4 \times 3 \times 3}$ and $Z_5 \in \mathbb{R}^{1 \times 4 \times 3 \times 3}$. Moreover, D_c and D_s are channel and spatial descriptors are defined as follows:

$$\begin{cases} D_c = \frac{1}{H \times W} \sum_{i=1}^H \sum_{j=1}^W X(i, j)_k \quad k=1,2,\dots,C \\ D_s = \frac{1}{C} \sum_{k=1}^C X(k)_{i,j} \quad i=1,2,\dots,H, \quad j=1,2,\dots,W \end{cases} \quad (4)$$

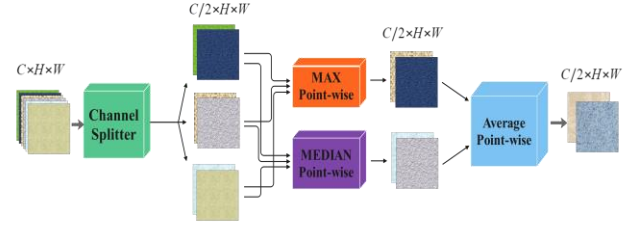


Fig. 2. The illustration of PWFS block.

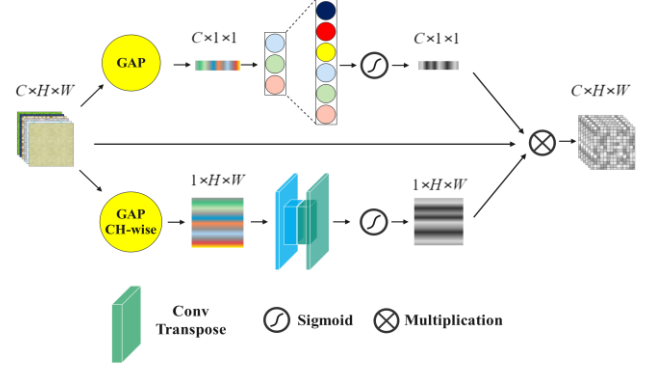


Fig. 3. The structure of our MassAtt module.

IV. EXPERIMENTS

We conducted a series of experiments to evaluate and compare the performance of the proposed model. For this purpose, we used FER datasets, namely KDEF, FER-2013 and FERPlus.

A. Datasets

Three well-known datasets, KDEF, FER-2013 and FER+, were employed to evaluate the performance of our proposed models.

KDEF [17] contains 4900 RGB images with corresponding labels, which have balanced distribution among each expression of disgust, anger, fear, happy, surprise, sad, and neutral. Each expression was expressed by 70 actors in 5 different multi-view angles (-90° , -45° , 0° , 45° and 90°). Some examples are illustrated in Fig. 4.

FER-2013 [18] was introduced in ICML-2013 challenge. The Google image search API was employed to find facial images using a set of 184 keywords that are related to emotions. After rejecting the incorrectly labeled images, each image was cropped and resized to 48×48 . FER-2013 contains 35887 grayscale images with corresponding labels, distributed as 4953 angry, 547 disgust, 5121 fear, 8989 happy, 4002 surprise, 6077 sad, and 6198 neutral. The dataset consists of 28,709 training samples and 7,178 test samples, equally divided between validation and test sets.

FERPlus [19] is a modified version of FER-2013, where the labels were improved using crowdsourcing. Therefore, 10 taggers were asked to label the images into eight classes: neutral (Ne), happy (Ha), surprise (Su), sad (Sa), angry (An), disgust (Di), fear (Fe), and contempt (Co). It is notable that we considered the majority of each sample tags as a final label. The dataset consists of 25,371 training samples, 3,225 validation

samples, and 3,160 private test images. Samples of FER-2013 and FERPlus are shown in Fig. 5.

We evaluated our model on *Pose-FERPlus* dataset to demonstrate its robustness under variant poses. This dataset is a subset of FERPlus collected by [9] including samples with poses greater than 30° and 45°. In addition, we utilize the indexes provided by [9] for samples with poses larger than 30° and 45° to introduce the *Pose-FER-2013* dataset.



Fig. 4. Samples of facial expression images from KDEF dataset.



Fig. 5. Samples of facial expression images from FER-2013 [18] and FERPlus [19].

B. Experimental Setup

The input images were first resized to 64×64 pixel and normalized using min-max normalization. Subsequently, three data augmentation techniques (image cropping, rotation and flipping) were employed to expand the training set, resulting in three supplementary synthetic 64×64 images for each original image.

We employ 5-fold cross-validation in KDEF dataset, since it does not specify the test set. The proposed model was implemented using TensorFlow framework, and all experiments were conducted on Google Colab environment. The model was compiled with categorical cross-entropy loss and a batch size of 32. The weights between neurons were updated using Adam optimizer. The initial learning rate was set to 0.001 and decayed after every eight epochs if validation loss failed to improve.

Multiple evaluation metrics were employed to assess the performance of the model, including parameter counts, accuracy (Acc), information density (ID) [34], and variance of

accuracies (Var). The metric ID is defined as the ratio of accuracy to parameters (in million). This metric indicates the degree to which a model employs its parameters efficiency to achieve a specific level of accuracy. Therefore, an architecture with high ID maintains high accuracy while having fewer parameters. Unlike previous literature that only considers accuracy to evaluate robustness to multi-view conditions, we calculate Var across different poses. A robust method to pose variation shows a slight degradation in accuracies for various poses, resulting in a low Var value.

C. Results and Discussion

1) Experiments on KDEF:

We conducted an experiment on KDEF dataset to assess the performances of LANMSFF in multi-view situations. Table II shows the LANMSFF’s recognition rate of each expression under multi-view scenarios on five poses. As we can see in this Table, our proposed model achieves 90.77% on the entire dataset. The robustness of the model against pose variation is clearly demonstrated by the negligible difference between the overall accuracy and the accuracy of each pose. These findings are in line with other studies [30], [35] which found that the 0° pose experiences the highest accuracy and the -90° pose reaches the lowest accuracy. A notable increase in accuracy is observed for “Neutral” and a significant decrease in accuracy is noted for “Disgust” when the viewpoint shifts from frontal to non-frontal. This observation implies that the model might struggle to capture critical facial features that are essential for accurate expression recognition from certain viewpoints. Table III displays the confusion matrix on KDEF dataset, showing “Happy” and “Neutral” achieve high accuracy, while “Fear” and “Disgust” experience lower accuracy. Specifically, “Fear” and “Disgust” expressions are prone to be confused with “surprise” and “Fear”, respectively.

TABLE II
RECOGNITION ACCURACIES FOR MULTI-VIEW IMAGES ON
KDEF DATASET

Pose	ACC (%)							
	Whole	An	Di	Fe	Ha	Sa	Su	Ne
-90°	89.44	87.02	82.52	82.92	99.26	85.03	90.78	98.57
-45°	91.18	89.97	88.33	81.46	97.83	89.40	92.87	98.59
0°	92.04	89.84	97.06	80.62	99.31	88.36	92.79	95.71
45°	91.00	88.53	90.55	79.91	99.26	87.87	92.12	98.54
90°	90.17	89.28	88.50	77.92	97.88	85.74	95.71	96.47
Overall	90.77	88.93	89.39	80.57	98.70	87.28	92.85	97.58

TABLE III
THE NORMALIZED CONFUSION MATRIX ON KDEF DATASET

Actual	Predict							
	Fe	An	Di	Ha	Ne	Sa	Su	Ne
Fe	80.60	1.69	1.46	1.29	1.15	6.87	6.94	
An	1.99	88.95	4.34	1.57	1.28	1.87	0	
Di	2.46	3.18	89.44	1.59	0.15	3.18	0	
Ha	0.43	0.14	0.57	98.72	0.14	0	0	
Ne	0.15	0.71	0	0	97.57	1.57	0	
Sa	4.13	1.44	2.57	0.57	3.82	87.33	0.14	
Su	6.14	0	0	0.15	0.72	0.29	92.70	

2) Experiments on FER-2013:

As shown in Table IV, LANMSFF achieves an average accuracy of 70.44% across the entire FER-2013 test set. However, the accuracy decreases for test set images with non-frontal images. These observed difficulties in recognition rate can be attributed to the challenging nature of the in-the-wild images in FER-2013 dataset. Table V displays the confusion matrix for FER-2013, revealing a low recognition rate for “Fear” and “Sadness”, with confusion between “Fear- Sadness” and “Sadness-Neutral”. This issue can be justified by false tag, non-facial samples, and imbalanced classes in this dataset. Table VI demonstrates that our model performance exceeds other methods (e.g., [21], [36], [37], [38], [39], [40], [41], [42]) on FER-2013 dataset, particularly when considering ID metric. Block-FreNet [39] uses frequency domain for feature extraction, BReG-NeXt [37] utilizes a complex function instead of identity mapping in shortcut path of residual blocks. LANMSFF achieves a notable ID by significantly reducing the number of parameters, albeit with a little trade-off in accuracy compared to existing approaches in the literature that report higher accuracy. For instance, although AMP_NET [42] achieves a higher accuracy of 4% than our model, its usage of 276 times more parameters leads to a diminished ID.

TABLE IV
RECOGNITION RATE UNDER MULTI-VIEW POSE ON FER-2013 AND POSE-FER-2013 DATASETS

Pose	ACC (%)							
	Whole	An	Di	Fe	Ha	Sa	Su	Ne
>30°	69.15	63.74	75.00	37.33	88.89	55.71	82.20	76.00
>45°	66.82	59.34	75.00	37.97	85.21	59.31	82.14	71.55
Overall	70.44	62.12	74.55	45.08	89.42	54.71	80.53	79.55

TABLE V
THE NORMALIZED CONFUSION MATRIX ON FER-2013

		Predict						
		Fe	An	Di	Ha	Ne	Sa	Su
Actual	Fe	62.12	1.43	8.35	3.25	12.42	1.43	11.00
	An	18.17	74.55	0	0	1.82	3.64	1.82
	Di	13.06	1.14	45.08	2.65	17.05	8.71	12.31
	Ha	1.02	0	0.35	89.42	2.39	2.50	4.32
	Ne	9.09	0.51	8.75	4.21	54.71	1.18	21.55
	Sa	2.64	0.48	7.93	4.58	1.44	80.53	2.40
	Su	3.83	0.16	2.40	3.51	9.11	1.44	79.55

TABLE VI
COMPARISON OF ACCURACY (%) AND PARAMETERS COUNTS BETWEEN PROPOSED METHOD AND PREVIOUS WORKS ON FER-2013

Methods	Acc (%)	Params	ID
SHCNN [36]	69.10	8700K	7.9
Light CNN [21]	68.00	1108K	61.3
BReG-NeXt-32 [37]	69.11	1900K	36.37
BReG-NeXt-50 [37]	71.53	3100K	23.07
Dense_FaceLiveNet [38]	69.99	15300K	4.57
Block-FreNet [39]	64.41	9000K	7.16
SAN-CNN [40]	74.17	6580K	11.2
AR-TE-CATFFNet [41]	74.84	32117K	2.3
AMP_NET [42]	74.48	105670K	0.7
LANMSFF	70.44	358K	196

3) Experiments on FERPlus:

The performance of LANMSFF on FERPlus is displayed in Table VII, demonstrating an average accuracy of 86.96% for

the complete test dataset. However, the accuracy of the model decreases when confronted images with >45° and >30° poses, consistent with the results seen in the existing approaches. Table VIII depicts the confusion matrix on FERPlus. The results indicate that “Neutral” and “Happiness” demonstrate the most accurate prediction, whereas “Contempt”, “Disgust”, and “Fear” exhibit inaccuracies. Insufficient samples for “Contempt”, “Disgust”, and “Fear” make these three classes more difficult to distinguish and prone to misclassification as “Neutral”, “Angry”, and “Surprise”, respectively. Considering the discrepancies in prediction accuracy across these classes, the class imbalance distribution cannot be overlooked. The number of samples directly affects the model’s ability to learn features, since there is a positive correlation between a large quantity of “Neutral” and “Happiness” samples with their high accuracy. Table IX depicts the comparison of our model with SOTA methods, including FENN [43] utilizing an approach to mitigate feature and label noise, TST-RNN [10] based on representation reinforcement network and transfer self-training. Our results indicate that a substantial reduction in model parameters results in a significant ID, albeit with a slight decrease in accuracy, compared to certain methods in the literature. As an illustration, our accuracy is marginally 3% lower compared to FENN [43] and PACVT [27], which have 30 and 74 times more parameters than our model, respectively.

TABLE VII
RECOGNITION RATE UNDER MULTI-VIEW POSE ON FERPLUS AND POSE-FERPLUS DATASETS

Pose	ACC (%)								
	Whole	Ne	Ha	Su	Sa	An	Di	Fe	Co
>30°	86.92	90.3	94.4	88.9	72.8	86.2	20.0	50.0	0
>45°	84.68	88.1	93.6	88.1	69.6	80.7	100	50.0	0
Overall	86.96	89.3	94.9	89.0	71.9	85.5	43.7	55.8	13.3

TABLE VIII
THE NORMALIZED CONFUSION MATRIX ON FERPLUS

		Predict							
		Ne	Ha	Su	Sa	An	Di	Fe	Co
Actual	Ne	89.38	2.12	1.11	6.28	0.74	0.09	0.28	0
	Ha	2.46	94.96	1.35	1.01	0.22	0	0	0
	Su	4.31	1.78	89.09	1.02	1.52	0	2.28	0
	Sa	20.68	2.36	0.78	71.99	3.14	0	1.05	0
	An	5.95	4.46	1.49	1.86	85.50	0.37	0.37	0
	Di	6.25	6.25	12.5	0	31.25	43.75	0	0
	Fe	3.48	0	27.91	10.47	2.33	0	55.81	0
	Co	46.67	6.67	0	20	13.33	0	0	13.33

TABLE IX
COMPARISON OF ACCURACY (%) AND PARAMETERS COUNTS BETWEEN PROPOSED METHOD AND PREVIOUS WORKS ON FERPLUS

Methods	Acc (%)	Params	ID
SHCNN [36]	86.50	8700K	9.94
FENN [43]	89.53	11470K	7.80
PACVT [27]	88.72	28400K	3.1
TST-RRN [10]	89.64	1820K	49.25
RAN [9]	89.16	11180K	7.94
CERN [20]	88.17	1450K	60.8
VTFE [28]	88.81	80000K	1.1
LANMSFF	86.96	358K	242

4) Robustness Analysis to multi-view poses:

Table X demonstrates that our proposed model achieves higher accuracy than SOTA methods, including DML-NET [30] employing dynamic constraint multi-task learning to estimate head poses as an additional task, and SSA-Net [44], which utilizes both an attention mechanism and dynamic constraint multi-task learning. OCA-MTL [35] achieves an accuracy of 89.04% using both frontal and non-frontal images as inputs for the Siamese network, which is 1.73% lower than the accuracy of our method. In contrast to our approach, they rely only on channel attention to focus on salient facial regions. Our Var is 0.66, compared to 3.69 for DML-NET [30], 5.42 for SSA-Net [44], and 2.74 for OCA-MTL [35]. The obtained outcomes validate the robustness of our suggested approach when applied to non-frontal images.

Our work is contrasted with SOTA methods in Table XI, which includes CERN [20], RAN [9], AMP_NET [42], VTFF [28], and FG-AGR [45] on Pose-FERPlus. This table computes Var for $\text{Pose} \geq 30^\circ$, $\text{Pose} \geq 45^\circ$, and the entire dataset to evaluate the robustness of each method to head-pose variations. Our model achieved a Var value of 1.13, compared to 1.88 for CERN, 2.31 for FG-AGR, and 14.2 for RAN methods. Our lower Var demonstrates enhanced robustness to head-pose variation in comparison to prior studies.

TABLE X
COMPARISON OF ACCURACIES BETWEEN THE PROPOSED METHOD AND PREVIOUS WORKS ON KDEF

Methods	Acc (%)					Overall	Var
	-90°	-45°	0°	+45°	+90°		
DML-NET [30]	89.20	88.80	91.30	85.60	86.10	88.20	3.69
SSA-Net [44]	90.20	90.20	89.70	83.50	89.10	88.50	5.42
OCA-MTL [35]	87.04	89.18	92.24	89.18	87.55	89.04	2.74
LANMSFF	89.44	91.18	92.04	91.00	90.17	90.77	0.66

TABLE XI
COMPARISON OF ACCURACIES BETWEEN THE PROPOSED METHOD AND PREVIOUS WORKS ON POSE-FERPLUS

Methods	Acc (%)			Var
	Pose $\geq 30^\circ$	Pose $\geq 45^\circ$	Overall	
RAN [9]	82.23	80.40	89.16	14.23
CERN [20]	86.84	84.83	88.17	1.88
FG-AGR [45]	88.38	87.52	91.09	2.31
AMP_NET [42]	88.52	87.57	-	-
VTFF [28]	88.29	87.20	88.81	0.45
LANMSFF	86.92	84.68	86.96	1.13

D. Visualization

Fig. 6 utilizes Grad-CAM [46] tool to visualize activation maps of our model. It shows that the model highlights salient facial features, including the eyes, mouth, and nose, even in multi-view scenarios.

E. Ablation Study

Table XII presents an ablation study that investigates the impact of the MassAtt and PWFS modules on robustness to multi-view poses. To this end, we evaluate four models with different configurations: whole model, whole model without PWFS, whole model without MassAtt, and whole model

without PWFS and MassAtt on KDEF dataset. The results clearly indicate the significance of these modules. Specifically, the absence of each module results in a 0.4 increase in Var for PWFS and a 1.94 increase for MassAtt. In addition, the removal of both modules simultaneously leads to a 1-point rise in Var and a decrease in overall accuracy. This illustrates that both the proposed PWFS and MassAtt modules contributed to improving the performance of LANMSFF on multi-view poses by removing weak features and concentrating on key ones, respectively.



Fig. 6. Activation maps visualization using Grad-Cam. Salient regions are depicted in warm colors (e.g., red and yellow), while less important regions are represented with cold colors (e.g., blue and green).

TABLE XII
ABLATION STUDY ON TEST SET OF KDEF DATASET

Methods	Acc (%)					Overall	Var
	-90°	-45°	0°	45°	90°		
Whole model	89.44	91.18	92.04	91.00	90.17	90.77	0.66
Whole model without PWFS	89.85	91.28	92.05	92.84	90.16	91.24	1.05
Whole model without MassAtt	87.59	91.59	92.15	92.43	90.38	90.83	2.59
Whole model without MassAtt and PWFS	89.14	90.57	91.75	92.53	88.93	90.58	1.65

V. CONCLUSION

This article presented LANMSFF to mitigate the challenges of high computational complexity and multi-view variations by suggesting a network based on lightweight FCN including MassAtt and PWFS blocks to tackle multi-view head pose. We employed MassAtt block as an attention mechanism which generated spatial and channel attention maps to emphasize relevant features. Furthermore, PWFS module as a multi-scale feature selector was utilized to remove weak features before fusion of multi-scale feature, unlike direct fusion in many existing methods. Experiments were conducted on KDEF, FER-2013, and FERPlus datasets. The results demonstrate that the model is robust to head-pose variation and achieves accuracy levels comparable to existing methods, using few parameters. Our future research will focus on dynamic datasets, incorporating spatiotemporal samples. In addition, we plan to incorporate pose estimation as a supplementary task.

REFERENCES

- [1] Z. Zeng, M. Pantic, G. I. Roisman, and T. S. Huang, "A survey of affect recognition methods: Audio, visual, and spontaneous expressions," *IEEE Trans. Pattern Anal. Mach. Intell.*, vol. 31, no. 1, pp. 39–58, 2009.
- [2] P. Ekman and W. V. Friesen, "Constants across cultures in the face and emotion," *J. Pers. Soc. Psychol.*, vol. 17, no. 2, pp. 124–129, Feb. 1971.
- [3] Y. Xia, H. Yu, X. Wang, M. Jian, and F. Y. Wang, "Relation-Aware Facial Expression Recognition," *IEEE Trans. Cogn. Dev. Syst.*, vol. 14, no. 3, pp. 1143–1154, 2022.
- [4] A. Krizhevsky, I. Sutskever, and G. E. Hinton, "ImageNet classification with deep convolutional neural networks," *Commun. ACM*, vol. 60, no. 6, pp. 84–90, 2017.
- [5] K. Simonyan and A. Zisserman, "Very deep convolutional networks for large-scale image recognition," *arXiv Prepr. arXiv1409.1556*, 2014.
- [6] A. G. Howard *et al.*, "MobileNets: Efficient Convolutional Neural Networks for Mobile Vision Applications," *arXiv Prepr. arXiv 1704.04861v1*, Apr. 2017.
- [7] C. Szegedy *et al.*, "Going deeper with convolutions," in *Proc. IEEE Comput. Soc. Conf. Comput. Vis. Pattern Recognit.*, 2015.
- [8] N. Sun, J. Tao, J. Liu, H. Sun, and G. Han, "3-D Facial Feature Reconstruction and Learning Network for Facial Expression Recognition in the Wild," *IEEE Trans. Cogn. Dev. Syst.*, vol. 15, no. 1, pp. 298–309, 2023.
- [9] K. Wang, X. Peng, J. Yang, D. Meng, and Y. Qiao, "Region Attention Networks for Pose and Occlusion Robust Facial Expression Recognition," *IEEE Trans. Image Process.*, vol. 29, pp. 4057–4096, 2020.
- [10] C.-S. Jiang, Z.-T. Liu, M. Wu, J. She, and W.-H. Cao, "Efficient Facial Expression Recognition With Representation Reinforcement Network and Transfer Self-Training for Human-Machine Interaction," *IEEE Trans. Ind. Informatics*, vol. 19, no. 9, pp. 9943–9952, 2023.
- [11] Q. Huang, C. Huang, X. Wang, and F. Jiang, "Facial expression recognition with grid-wise attention and visual transformer," *Inf. Sci.*, vol. 580, pp. 35–54, 2021.
- [12] S. Woo, J. Park, J. Y. Lee, and I. S. Kweon, "CBAM: Convolutional block attention module," in *Proc. Eur. Conf. Comput. Vis.*, 2018, pp. 3–19.
- [13] J. Hu, L. Shen, S. Albanie, G. Sun, and E. Wu, "Squeeze-and-Excitation Networks," *IEEE Trans. Pattern Anal. Mach. Intell.*, vol. 42, no. 8, pp. 2011–2023, 2020.
- [14] Z. Zhao, Q. Liu, and S. Wang, "Learning Deep Global Multi-Scale and Local Attention Features for Facial Expression Recognition in the Wild," *IEEE Trans. Image Process.*, vol. 30, pp. 6544–6556, 2021.
- [15] Y. Fan, V. O. K. Li, and J. C. K. Lam, "Facial Expression Recognition with Deeply-Supervised Attention Network," *IEEE Trans. Affect. Comput.*, vol. 13, no. 2, pp. 1057–1071, 2022.
- [16] J. Xiao, C. Gan, Q. Zhu, Y. Zhu, and G. Liu, "CFNet: Facial expression recognition via constraint fusion under multi-task joint learning network," *Appl. Soft Comput.*, vol. 141, p. 110312, 2023.
- [17] M. G. Calvo and D. Lundqvist, "Facial expressions of emotion (KDEF): Identification under different display-duration conditions," *Behav. Res. Methods*, vol. 40, no. 1, pp. 109–115, 2008.
- [18] I. J. Goodfellow *et al.*, "Challenges in representation learning: A report on three machine learning contests," *Neural Netw.*, vol. 64, pp. 59–63, 2015.
- [19] E. Barsoum, C. Zhang, C. C. Ferrer, and Z. Zhang, "Training deep networks for facial expression recognition with crowd-sourced label distribution," in *Proc. 18th ACM Int. Conf. Multimodal Interact., ICMI 2016*, 2016, pp. 279–283.
- [20] D. Gera, S. Balasubramanian, and A. Jami, "CERN: Compact facial expression recognition net," *Pattern Recognit. Lett.*, vol. 155, pp. 9–18, 2022.
- [21] J. Shao and Y. Qian, "Three convolutional neural network models for facial expression recognition in the wild," *Neurocomputing*, vol. 355, pp. 82–92, 2019.
- [22] X. Wu, R. He, Z. Sun, and T. Tan, "A light CNN for deep face representation with noisy labels," *IEEE Trans. Inf. Forensics Secur.*, vol. 13, no. 11, pp. 2884–2896, 2018.
- [23] Q. Wang, B. Wu, P. Zhu, P. Li, W. Zuo, and Q. Hu, "ECA-Net: Efficient channel attention for deep convolutional neural networks," in *Proc. IEEE Comput. Soc. Conf. Comput. Vis. Pattern Recognit.*, 2020, pp. 11531–11539.
- [24] G. Huang, Z. Liu, L. van der Maaten, and K. Q. Weinberger, "Densely Connected Convolutional Networks," in *Proc. IEEE Comput. Soc. Conf. Comput. Vis. Pattern Recognit.*, 2017, pp. 4700–4708.
- [25] J. Li, K. Jin, D. Zhou, N. Kubota, and Z. Ju, "Attention mechanism-based CNN for facial expression recognition," *Neurocomputing*, vol. 411, pp. 340–350, 2020.
- [26] Y. Li, G. Lu, J. Li, Z. Zhang, and D. Zhang, "Facial Expression Recognition in the Wild Using Multi-Level Features and Attention Mechanisms," *IEEE Trans. Affect. Comput.*, vol. 14, no. 1, pp. 451–462, 2023.
- [27] C. Liu, K. Hirota, and Y. Dai, "Patch attention convolutional vision transformer for facial expression recognition with occlusion," *Inf. Sci.*, vol. 619, pp. 781–794, 2023.
- [28] F. Ma, B. Sun, and S. Li, "Facial Expression Recognition With Visual Transformers and Attentional Selective Fusion," *IEEE Trans. Affect. Comput.*, vol. 14, no. 2, pp. 1236–1248, 2023.
- [29] M. Jampour and M. Javidi, "Multiview Facial Expression Recognition, A Survey," *IEEE Trans. Affect. Comput.*, vol. 13, no. 4, pp. 2086–2105, 2022.
- [30] Y. Liu *et al.*, "Dynamic multi-channel metric network for joint pose-aware and identity-invariant facial expression recognition," *Inf. Sci.*, vol. 578, pp. 195–213, 2021.
- [31] K. He, X. Zhang, S. Ren, and J. Sun, "Deep residual learning for image recognition," in *Proc. IEEE Comput. Soc. Conf. Comput. Vis. Pattern Recognit.*, 2016, pp. 770–778.
- [32] F. Yu and V. Koltun, "Multi-scale context aggregation by dilated convolutions," in *4th Int. Conf. Learn. Represent. ICLR 2016*, 2016.
- [33] R. R. Adyapada and B. Annappa, "A comprehensive review of facial expression recognition techniques," *Multimed. Syst.*, vol. 29, no. 1, pp. 73–103, 2023.
- [34] A. Canziani, A. Paszke, and E. Culurciello, "An Analysis of Deep Neural Network Models for Practical Applications," *arXiv Prepr. arXiv1605.07678*, 2016.
- [35] J. Chen, L. Yang, L. Tan, and R. Xu, "Orthogonal channel attention-based multi-task learning for multi-view facial expression recognition," *Pattern Recognit.*, vol. 129, p. 108753, 2022.
- [36] S. Miao, H. Xu, Z. Han, and Y. Zhu, "Recognizing facial expressions using a shallow convolutional neural network," *IEEE Access*, vol. 7, pp. 78000–78011, 2019.
- [37] B. Hasani, P. S. Negi, and M. H. Mahoor, "BRcG-NeXt: Facial Affect Computing Using Adaptive Residual Networks with Bounded Gradient," *IEEE Trans. Affect. Comput.*, vol. 13, no. 2, pp. 1023–1036, 2022.
- [38] J. C. Hung, K. C. Lin, and N. X. Lai, "Recognizing learning emotion based on convolutional neural networks and transfer learning," *Appl. Soft Comput.*, vol. 84, p. 105724, Nov. 2019.
- [39] Y. Tang, X. Zhang, X. Hu, S. Wang, and H. Wang, "Facial Expression Recognition Using Frequency Neural Network," *IEEE Trans. Image Process.*, vol. 30, pp. 444–457, 2021.
- [40] M. D. Putro, D. L. Nguyen, and K. H. Jo, "A Fast CPU Real-Time Facial Expression Detector Using Sequential Attention Network for Human-Robot Interaction," *IEEE Trans. Ind. Informatics*, vol. 18, no. 11, pp. 7665–7674, 2022.
- [41] M. Sun *et al.*, "Attention-Rectified and Texture-Enhanced Cross-Attention Transformer Feature Fusion Network for Facial Expression Recognition," *IEEE Trans. Ind. Informatics*, vol. 19, no. 12, pp. 11823–11832, 2023.
- [42] H. Liu, H. Cai, Q. Lin, X. Li, and H. Xiao, "Adaptive Multilayer Perceptual Attention Network for Facial Expression Recognition," *IEEE Trans. Circuits Syst. Video Technol.*, vol. 32, no. 9, pp. 6253–6266, 2022.
- [43] Y. Gu, H. Yan, X. Zhang, Y. Wang, Y. Ji, and F. Ren, "Towards Facial Expression Recognition in the Wild via Noise-tolerant Network," *IEEE Trans. Circuits Syst. Video Technol.*, vol. 33, no. 5, pp. 2033–2047, Nov. 2023.
- [44] Y. Liu, J. Peng, W. Dai, J. Zeng, and S. Shan, "Joint spatial and scale attention network for multi-view facial expression recognition," *Pattern Recognit.*, vol. 139, p. 109496, 2023.
- [45] C. Li, X. Li, X. Wang, D. Huang, Z. Liu, and L. Liao, "FG-AGR: Fine-Grained Associative Graph Representation for Facial Expression Recognition in the Wild," *IEEE Trans. Circuits Syst. Video Technol.*, vol. 34, no. 2, pp. 882–896, 2023.
- [46] R. R. Selvaraju, M. Cogswell, A. Das, R. Vedantam, D. Parikh, and D. Batra, "Grad-CAM: Visual Explanations from Deep Networks via Gradient-Based Localization," in *2017 IEEE Int. Conf. Comput. Vis.*, 2017, pp. 618–626.